Suppressing cross-talk for elastic FWI with multi-parameter approximate Hessian and its parameter-type approximation

Wenyong Pan, Kris Innanen

ABSTRACT

Full Waveform Inversion (FWI) method becomes popular in recent years for estimating subsurface parameters by iteratively minimizing the difference between the modelled data and observed data. Inverting isotropic and elastic parameters using multi-parameter FWI has been studied by many researchers. While updating multiple parameters is still a challenging problem for increasing the nonlinearity of the inverse problem. One difficulty for multi-parameter FWI is known as cross-talk problem rising from the coupling effects between different physical parameters. It is known that the strong coupling effects between P-wave velocity and density make it difficult to recover density. In this research, we examine the ability of multi-parameter approximate Hessian and its parameter-type approximation in suppressing cross-talk and de-coupling the elastic parameters. We also show that they can be calculated using adjoint-state technique efficiently. Compared to the multi-parameter approximate Hessian, the parameter-type approximation can be inverted trivially and its storage requirement is reduced greatly.

INTRODUCTION

Full Waveform Inversion (FWI) estimates the subsurface parameters by iteratively minimizing the difference between the modelled data and observed data (Lailly, 1983; Tarantola, 1984). In recent years, it is widely studied by many geophysicists in academic and industrial level. Inversing multiple parameters using FWI makes the inverse problem more undetermined. Furthermore, multi-parameter FWI also suffers from the cross-talk (or trade-off) problem rising from the coupling effects between different physical parameters, which gives rise to the parameterization issue for multi-parameter FWI.

Estimating the isotropic and elastic parameters has been investigated by many researchers. Tarantola et al. (1985) originally analyzed the scattering patterns of different elastic parameters and emphasized the importance of parameterization choice for effective inversion. Mora (1987) carried out a nonlinear elastic FWI with multi-component data using preconditioned conjugate gradient algorithm. They found that for reflection seismic acquisition geometry, the impedance and velocity parameterizations are more suitable for inversion than Lamé parameterization. What's more, the similarity of the scattering patterns between P-wave velocity and density at shot apertures makes that density cannot be well resolved. The study of Köhn et al. (2012) reals a strong requirement of sequential inversion from low to high frequencies to reconstruct the density model.

The Hessian matrix $\mathbf{H}$ indicates the second-order partial derivative of the misfit function. The mono-parameter Hessian in mono-parameter FWI works as deconvolution operator for compensating the geometrical spreading and de-blurring the gradient (Pratt et al., 1998; Pan et al., 2014a,b). The multi-parameter Hessian has a block structure and carries more information. Newton's method requires the computation and inversion of the full

Hessian matrix, which is extremely expensive for large scale inverse problem. The conjugate gradient (CG) algorithms involve the Hessian-vector product for avoiding explicitly constructing and storing the Hessian. A number of CG iterations can achieve comparable inversion result compared to one obtained by Newton's method. The Quasi-Newton methods (e.g., l-BFGS method) approach the inverse Hessian iteratively by storing the changes of the gradient and model from a number of previous iterations.

The multi-parameter approximate Hessian $\tilde{\mathbf{H}}$ within Gauss-Newton method keeps the first-order term of full Hessian and its off-diagonal blocks indicate the correlation of Fréchet derivative wavefields with respect to different physical parameters and predict the coupling effects. Hence, the multi-parameter approximate Hessian $\tilde{\mathbf{H}}$ plays a crucial role in mitigating the cross-talk problem (Operto et al., 2013; Innanen, 2014c). However, efficient calculation, storage and inverting of $\tilde{\mathbf{H}}$ is still a challenging problem. Innanen (2014c) gave the parameter-type multi-parameter Hessian approximation $\tilde{\mathbb{H}}$, which keeps the diagonal elements of the block matrices and can also suppress cross-talk. In this research, we show that the multi-parameter approximate Hessian $\tilde{\mathbf{H}}$ and its parameter-type approximation $\tilde{\mathbb{H}}$ can also be constructed using adjoint-state technique. The additional forward modelling problems need to be solved is just equivalent to the number of receivers. Furthermore, $\tilde{\mathbb{H}}$ can be trivially inverted and its storage requirement is greatly reduced compared to that of $\tilde{\mathbf{H}}$.

The paper is organized as follows. First, we review the forward modelling problem in isotropic and elastic media and the basic theory of FWI. We then, introduce the multi-parameter approximate Hessian $\tilde{\mathbf{H}}$ and its parameter-type approximation $\tilde{\mathbb{H}}$. The expressions for calculating gradient vectors, $\tilde{\mathbf{H}}$ and $\tilde{\mathbb{H}}$ using adjoint-state method are given. In the numerical section, we verify the effectiveness of $\tilde{\mathbf{H}}$ and $\tilde{\mathbb{H}}$ in reducing cross-talk with a multi-scatter example. Then, the proposed method is applied on a modified Marmousi-II model.

THEORY AND METHODS

Elastic Full Waveform Inversion

Forward Modelling

The equation of motion for isotropic and elastic media is given by:

$$(\lambda + 2\mu)\,\nabla\nabla\cdot\mathbf{u} - \mu\nabla\times\nabla\times\mathbf{u} + \mathbf{f} = \rho\partial_t^2\mathbf{u}, \tag{1}$$

where λ and μ are Lamé constants, ρ is density, $\mathbf{f}$ is the force term with both a vertical source and a horizontal source, $\mathbf{u}$ indicates the displacement field. The P-wave velocity and S-wave velocity can be calculated as $\alpha = \sqrt{(\lambda + 2\mu)/\rho}$ and $\beta = \sqrt{\mu/\rho}$. The wavefields solutions are obtained using an explicit finite-difference method with fourth-order accuracy in space and second-order accuracy in time (Virieux, 1986; Levander, 1988). A Clayton Engquist boundary condition is applied on four boundaries of the model (Clayton and Engquist, 1980).

Basic Theory of FWI

Full waveform inversion (FWI) employs iterative scheme for inversing subsurface model parameter $\mathbf{m}$ to minimize the misfit Φ between the synthetic data $\mathbf{u}_{syn}$ and observed data $\mathbf{u}_{obs}$ (Lailly, 1983; Tarantola, 1984; Virieux and Operto, 2009). The misfit function is formulated as least-squares norm:

$$\Phi\left(\mathbf{m}\right) = \frac{1}{2}\|\mathbf{u}_{obs} - \mathbf{u}_{syn}\|_2^2, \tag{2}$$

where $\|\cdot\|_2$ means the ℓ-2 norm. The descent direction $\delta\mathbf{m}$ is the solution of Newton system:

$$\mathbf{H}_k\delta\mathbf{m}_k = -\nabla_m\Phi\left(\mathbf{m}_k\right), \tag{3}$$

where k is the iteration number, $\nabla_m\Phi\left(\mathbf{m}_k\right)$ and $\mathbf{H}_k$ are the gradient and Hessian, corresponding to the first and second-order partial derivative of the misfit function. Conjugate gradient (CG) methods avoids explicitly calculating and inversing the Hessian by involving Hessian-vector product. Quasi-Newton methods (e.g, l-BFGS method) approach the inverse Hessian iteratively by storing the change of the gradient and model from a number of previous iterations. Newton-like methods (e.g., Gauss-Newton method) tend to build approximate versions of Hessian matrix (Pratt et al., 1998). Inversing the isotropic and elastic parameters using FWI has been studied by many researchers (Epanomeritakis et al., 2008; Xiong et al., 2011; Köhn et al., 2012). While effective updating the multiple elastic parameters simultaneously is still a challenging task. The coupling effects between different physical parameters result in the cross-talk (trade-off) problem, which also give rise to the parameterization issue for elastic FWI (Tarantola, 1986). The overlap of Fréchet derivative wavefields due to different physical parameters at certain range of scattering angle mainly accounts for this problem (Operto et al., 2013).

Elastic multi-parameter approximate Hessian and its parameter-type approximation

For multi-parameter FWI, the Hessian matrix has a block structure with N_p diagonal blocks and $N_p(N_p-1)$ off-diagonal blocks, where N_p is the number physical parameters. The diagonal blocks correspond to second-order partial derivative of the misfit function with respect to the same physical parameter $\nabla_m\nabla_m\Phi$. The off-diagonal blocks correspond to second-order partial derivative of the misfit function with respect to different physical parameters $\nabla_m\nabla_{m'}\Phi$ ($m \neq m'$). The Gauss-Newton multi-parameter approximate Hessian $\tilde{\mathbf{H}}$ only keeps the first-order term in full Hessian by ignoring the second-order scattering effects. Considering Gauss-Newton elastic FWI with Lamé constants parameterization, equation (3) can be changed to:

$$\begin{bmatrix} \tilde{\mathbf{H}}_{\lambda\lambda} & \tilde{\mathbf{H}}_{\lambda\mu} & \tilde{\mathbf{H}}_{\lambda\rho} \\ \tilde{\mathbf{H}}_{\mu\lambda} & \tilde{\mathbf{H}}_{\mu\mu} & \tilde{\mathbf{H}}_{\mu\rho} \\ \tilde{\mathbf{H}}_{\rho\lambda} & \tilde{\mathbf{H}}_{\rho\mu} & \tilde{\mathbf{H}}_{\rho\rho} \end{bmatrix} \begin{bmatrix} \delta\mathbf{m}_\lambda \\ \delta\mathbf{m}_\mu \\ \delta\mathbf{m}_\rho \end{bmatrix} = - \begin{bmatrix} \nabla_\lambda\Phi \\ \nabla_\mu\Phi \\ \nabla_\rho\Phi \end{bmatrix}, \tag{4}$$

where $\nabla_\lambda\Phi$, $\nabla_\beta\Phi$, and $\nabla_\rho\Phi$ indicate the gradient vectors for parameters λ, μ, and ρ. The diagonal blocks of $\tilde{\mathbf{H}}$ are the correlations of two Fréchet derivative wavefields with respect

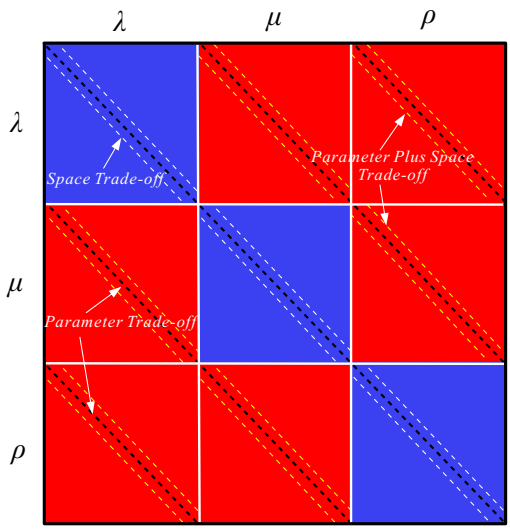

FIG. 1. Schematic diagram of the multi-parameter approximate Hessian $\tilde{\mathbf{H}}$ with elastic parameters λ, μ and ρ.

to the same physical parameter, as indicated by the blue boxes of Figure 1. The off-diagonal blocks are the correlation of two Fréchet derivative wavefields with respect to two different physical parameters, as indicated by the red boxes of Figure 1. For instance, the element $\tilde{\mathbf{H}}_{\lambda\lambda}(\mathbf{r},\mathbf{r}')$ in diagonal block $\tilde{\mathbf{H}}_{\lambda\lambda}$ and the element $\tilde{\mathbf{H}}_{\lambda\rho}(\mathbf{r},\mathbf{r}')$ in off-diagonal block $\tilde{\mathbf{H}}_{\lambda\rho}$ are:

$$\tilde{\mathbf{H}}_{\lambda\lambda}(\mathbf{r},\mathbf{r}') = \nabla_{\lambda(\mathbf{r})}\mathbf{u}^{\dagger}\nabla_{\lambda(\mathbf{r}')}\mathbf{u}^{*}, \tilde{\mathbf{H}}_{\lambda\rho}(\mathbf{r},\mathbf{r}') = \nabla_{\lambda(\mathbf{r})}\mathbf{u}^{\dagger}\nabla_{\rho(\mathbf{r}')}\mathbf{u}^{*}, \tag{5}$$

where the symbols $\dagger$ and $*$ indicate transpose and complex conjugate respectively. As shown in Figure 1, the off-diagonal elements in the diagonal blocks correspond to space-type trade-off. The diagonal elements in the off-diagonal blocks correspond to parameter-type trade-off. The off-diagonal elements of the off-diagonal blocks correspond to space-parameter-type trade-off. The off-diagonal blocks predict the coupling effects between different physical parameters and applying its inverse to the gradient can reduce the cross-talk.

Explicit calculation of Fréchet derivative wavefields needs number of $3N_g$ forward simulations, which is extremely expensive (N_g is the number of grid nodes). Furthermore, storing and inversing the approximate Hessian is also a challenging problem. Innanen (2014c,b) gave the parameter-type multi-parameter Hessian approximation $\tilde{\mathbb{H}}$, which only keeps the diagonal elements of sub-block matrices, as indicated by the black-dash lines of Figure 1. Innanen (2014b) proved its effectiveness in suppressing cross-talk with an analytic example. Its diagonal block element $\tilde{\mathbb{H}}_{\lambda\lambda}(\mathbf{r})$ and off-diagonal block element $\tilde{\mathbb{H}}_{\lambda\rho}(\mathbf{r})$ are expressible as:

$$\tilde{\mathbb{H}}_{\lambda\lambda}(\mathbf{r}) = \nabla_{\lambda(\mathbf{r})}\mathbf{u}^{\dagger}\nabla_{\lambda(\mathbf{r})}\mathbf{u}^{*}, \tilde{\mathbb{H}}_{\lambda\rho}(\mathbf{r}) = \nabla_{\lambda(\mathbf{r})}\mathbf{u}^{\dagger}\nabla_{\rho(\mathbf{r})}\mathbf{u}^{*}. \tag{6}$$

What's more, this parameter-type approximation can be inverted trivially and memory requirement for storing $\tilde{\mathbb{H}}$ is reduced by $1.5N_g$ times compared to storing $\tilde{\mathbf{H}}$.

Constructing Gradient, Multi-parameter approximate Hessian and parameter-type approximation with adjoint-state method

Innanen (2014a) gave the three-term gradient vector and nine-term Hessian operator for multi-component elastic reflection FWI. In this section, we show that the gradient vector, multi-parameter approximate Hessian and its parameter-type approximation can be calculated using adjoint-state method.

We can first recall the equation describing the propagation of scattered wavefields due to the perturbations of density $\delta\rho$ and elastic constants δc_{ijkl}:

$$\partial_j \left(\tilde{c}_{ijkl}\partial_l \delta u_k\right) - \tilde{\rho}\partial_t^2 \delta u_i = \delta\rho\partial_t^2 \tilde{u}_i - \partial_j \delta M_{ij}, \tag{7}$$

where $\tilde{u}_i$ indicates the i component of the incident wavefields, $\delta M_{ij} = \delta c_{ijkl}\tilde{e}_{kl}$ is the equivalent moment tensor source, and $\tilde{e}_{kl}$ denote the strain components of the incident wave. The derivation of equation (7) can be found in Pan and Innanen (2015). When only considering the perturbations of isotropic and elastic parameters, the solution of equation (7) can be written as an integral formulation in frequency domain:

$$\begin{aligned}
\delta\bar{u}_n\left(\mathbf{r},\omega\right) = &\int_{\Omega(\mathbf{r}')}\int_{\omega'} \delta\rho\omega^2\tilde{u}_i\tilde{G}_{ni}(\mathbf{r},\omega;\mathbf{r}',\omega')d\Omega(\mathbf{r}')d\omega' \\
&- \int_{\Omega(\mathbf{r}')}\int_{\omega'} \delta\lambda\tilde{e}_{kl}\delta_{ij}\delta_{kl}\partial_j\tilde{G}_{ni}(\mathbf{r},\omega;\mathbf{r}',\omega')d\Omega(\mathbf{r}')d\omega' \\
&- \int_{\Omega(\mathbf{r}')}\int_{\omega'} \delta\mu\tilde{e}_{kl}\left(\delta_{ik}\delta_{kl}+\delta_{il}\delta_{jk}\right)\partial_j\tilde{G}_{ni}(\mathbf{r},\omega;\mathbf{r}',\omega')d\Omega(\mathbf{r}')d\omega',
\end{aligned} \tag{8}$$

where $\tilde{G}_{ni}(\mathbf{r},\omega;\mathbf{r}',\omega')$ indicates the Green's tensor in the unperturbed background medium due to the scattered source at position $\mathbf{r}' = (x', y', z')$. $\Omega\left(\mathbf{r}'\right)$ indicates the volume including all of the scattered sources. The Fréchet derivative wavefields recorded at receiver $\mathbf{r}_g$ for a source located at $\mathbf{r}_s$ due to model perturbations $\delta\lambda\left(\mathbf{r}\right)$, $\delta\mu\left(\mathbf{r}\right)$ and $\delta\rho\left(\mathbf{r}\right)$ are expressible as:

$$\begin{aligned}
\nabla_{\lambda(\mathbf{r})}\bar{u}_n\left(\mathbf{r}_g,\mathbf{r}_s,\omega\right) &= -\tilde{e}_{kl}\delta_{ij}\delta_{kl}\partial_j\tilde{G}_{ni}(\mathbf{r},\mathbf{r}_g,\omega), \\
\nabla_{\mu(\mathbf{r})}\bar{u}_n\left(\mathbf{r}_g,\mathbf{r}_s,\omega\right) &= -\tilde{e}_{kl}\left(\delta_{ik}\delta_{kl}+\delta_{il}\delta_{jk}\right)\partial_j\tilde{G}_{ni}(\mathbf{r},\mathbf{r}_g,\omega), \\
\nabla_{\rho(\mathbf{r})}\bar{u}_n\left(\mathbf{r}_g,\mathbf{r}_s,\omega\right) &= \omega^2\tilde{u}_i\left(\mathbf{r},\mathbf{r}_s,\omega\right)\tilde{G}_{ni}(\mathbf{r},\mathbf{r}_g,\omega),
\end{aligned} \tag{9}$$

where $\tilde{e}_{kl} = 1/2\left(\partial_l\tilde{u}_k\left(\mathbf{r},\mathbf{r}_s,\omega\right) + \partial_k\tilde{u}_l\left(\mathbf{r},\mathbf{r}_s,\omega\right)\right)$ denote the strain components of the incident wave. Considering 2D elastic case (x-z plane), the gradients for λ, μ and ρ are expressible as:

$$\begin{aligned}
&\nabla_{\lambda(\mathbf{r})}\Phi = \\
&-\left\langle\left(\partial_x\tilde{u}_x\left(\mathbf{r},\mathbf{r}_s,\omega\right)+\partial_z\tilde{u}_z\left(\mathbf{r},\mathbf{r}_s,\omega\right)\right)\left(\partial_x\tilde{u}_x^*(\mathbf{r},\mathbf{r}_g,\omega)+\partial_z\tilde{u}_z^*\left(\mathbf{r},\mathbf{r}_g,\omega\right)\right)\right\rangle,
\end{aligned} \tag{10}$$

$$\begin{aligned}
&\nabla_{\mu(\mathbf{r})}\Phi = \\
&-\left\langle\left(\partial_x\tilde{u}_x\left(\mathbf{r},\mathbf{r}_s,\omega\right)+\partial_z\tilde{u}_z\left(\mathbf{r},\mathbf{r}_s,\omega\right)\right)\left(\partial_z\tilde{u}_x^*\left(\mathbf{r},\mathbf{r}_g,\omega\right)+\partial_x\tilde{u}_z^*\left(\mathbf{r},\mathbf{r}_g,\omega\right)\right)\right\rangle \\
&-2\left\langle\left(\partial_x\tilde{u}_x\left(\mathbf{r},\mathbf{r}_s,\omega\right)\partial_x\tilde{u}_x^*\left(\mathbf{r},\mathbf{r}_g,\omega\right)+\partial_z\tilde{u}_z\left(\mathbf{r},\mathbf{r}_s,\omega\right)\partial_z\tilde{u}_z^*\left(\mathbf{r},\mathbf{r}_g,\omega\right)\right)\right\rangle,
\end{aligned} \tag{11}$$

$$\nabla_{\rho(\mathbf{r})}\Phi = \left\langle\omega^2\left(\tilde{u}_x\left(\mathbf{r},\mathbf{r}_s,\omega\right)\tilde{u}_x^*\left(\mathbf{r},\mathbf{r}_g,\omega\right)+\tilde{u}_z(\mathbf{r},\mathbf{r}_s,\omega)\,\tilde{u}_z^*\left(\mathbf{r},\mathbf{r}_g,\omega\right)\right)\right\rangle, \tag{12}$$

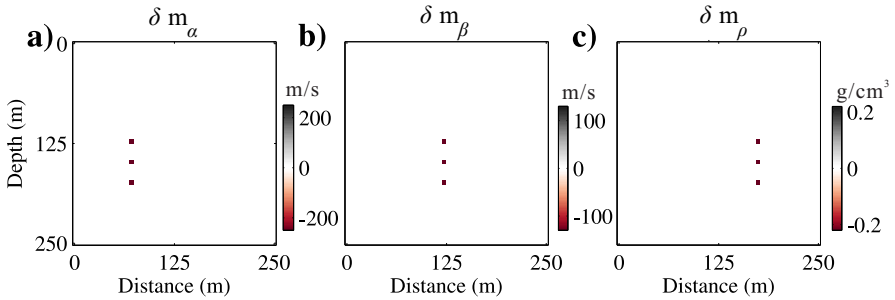

FIG. 2. (a), (b) and (c) show the true model perturbations $\delta\mathbf{m}_\alpha$, $\delta\mathbf{m}_\beta$ and $\delta\mathbf{m}_\rho$.

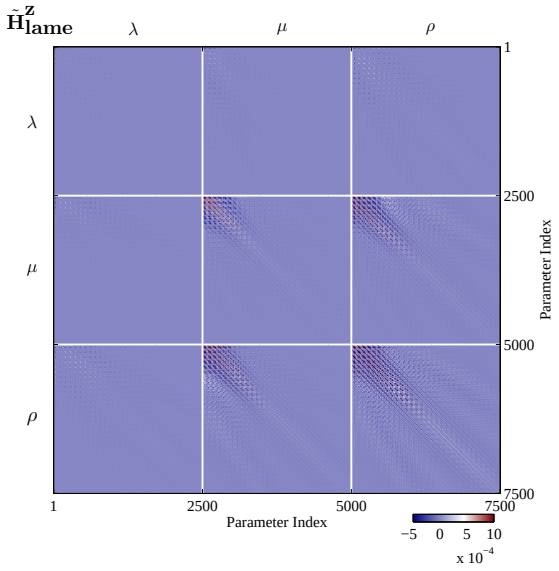

FIG. 3. The multi-parameter approximate Hessian $\tilde{\mathbf{H}}^{\mathbf{z}}_{\text{lame}}$ for Lamé constants parameterization (λ, μ and ρ) with z component data.

where $\langle\cdot\rangle$ means integration over $\mathbf{r}_s$, $\mathbf{r}_g$ and ω. $u_i^*(\mathbf{r},\mathbf{r}_g,\omega)$ indicate adjoint wavefields backpropagated from receiver $\mathbf{r}_g$ to $\mathbf{r}$:

$$u_i^*(\mathbf{r},\mathbf{r}_g,\omega) = \tilde{G}_{ni}(\mathbf{r},\mathbf{r}_g,\omega)\,\Delta d_n^*(\mathbf{r},\mathbf{r}_g,\omega), \tag{13}$$

where Δd_n indicate the n component of the data residuals. The gradient vectors for other parameterizations can be obtained using chain rule. For the Gauss-Newton multi-parameter approximate Hessian $\tilde{\mathbf{H}}$ in equation (4), its element is formed by correlating two Fréchet derivative wavefields:

$$\tilde{\mathbf{H}}_{mm'}(\mathbf{r},\mathbf{r}') = \nabla_{m(\mathbf{r})}\mathbf{u}^\dagger\nabla_{m'(\mathbf{r}')}\mathbf{u}^*. \tag{14}$$

Inserting the Fréchet derivative wavefields into equation (14), we can obtain the elements in all block matrices of $\tilde{\mathbf{H}}$. For instance, the elements $\tilde{\mathbf{H}}_{\lambda\lambda}(\mathbf{r},\mathbf{r}')$ and $\tilde{\mathbf{H}}_{\lambda\rho}(\mathbf{r},\mathbf{r}')$ are expressible as:

$$\begin{aligned}
&\tilde{\mathbf{H}}_{\lambda\lambda}(\mathbf{r},\mathbf{r}') = \\
&\partial_k\tilde{u}_k(\mathbf{r},\mathbf{r}_s,\omega)\,\partial_i\tilde{G}_{ni}(\mathbf{r},\mathbf{r}_g,\omega)\,\partial_k\tilde{u}_k^*(\mathbf{r}',\mathbf{r}_s,\omega)\partial_i\tilde{G}_{ni}^*(\mathbf{r}',\mathbf{r}_g,\omega),\\
&\tilde{\mathbf{H}}_{\lambda\rho}(\mathbf{r},\mathbf{r}') = \\
&-\omega^2\partial_k\tilde{u}_k(\mathbf{r},\mathbf{r}_s,\omega)\,\partial_i\tilde{G}_{ni}(\mathbf{r},\mathbf{r}_g,\omega)\,\tilde{u}_i^*(\mathbf{r}',\mathbf{r}_s,\omega)\,\tilde{G}_{ni}^*(\mathbf{r}',\mathbf{r}_g,\omega).
\end{aligned} \tag{15}$$

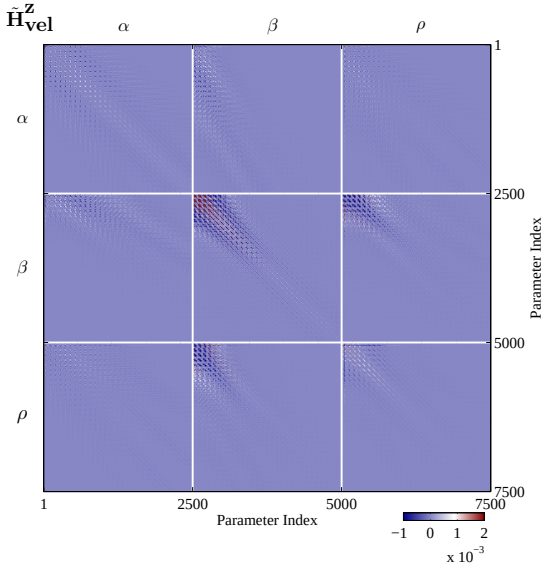

FIG. 4. The multi-parameter approximate Hessian $\tilde{\mathbf{H}}^{\mathbf{z}}_{\mathbf{vel}}$ for velocity parameterization (α, β and ρ) with z component data.

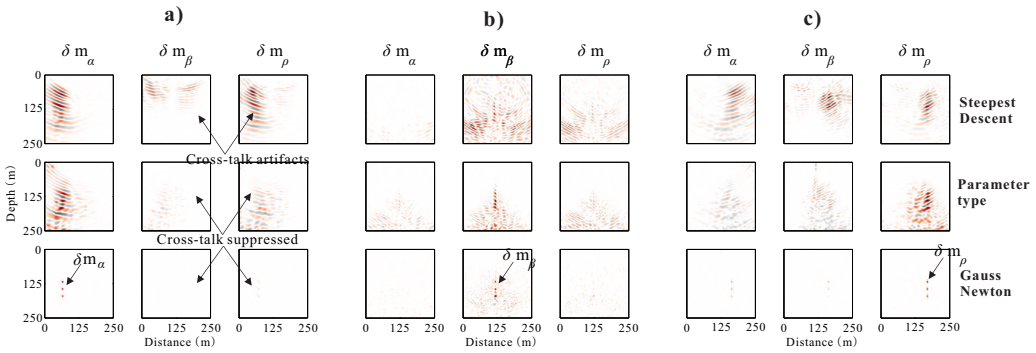

FIG. 5. The estimated model perturbations using steep descent method (the first row), parameter-type preconditioning method (the second row) and Gauss-Newton method (the third row) with data residuals $\Delta\mathbf{d}_\alpha$ (a), $\Delta\mathbf{d}_\beta$ (b) and $\Delta\mathbf{d}_\rho$ (c) respectively.

when $\mathbf{r} = \mathbf{r}'$, we can obtain the elements in parameter-type approximation $\tilde{\mathbb{H}}$. For instance:

$$\begin{aligned}
&\tilde{\mathbb{H}}_{\lambda\lambda}\left(\mathbf{r}\right) = \mid \partial_k \tilde{u}_k\left(\mathbf{r}, \mathbf{r}_s, \omega\right) \mid^2 \mid \partial_i \tilde{G}_{ni}\left(\mathbf{r}, \mathbf{r}_g, \omega\right) \mid^2, \\
&\tilde{\mathbb{H}}_{\lambda\rho}\left(\mathbf{r}\right) = \\
&-\omega^2 \partial_k \tilde{u}_k\left(\mathbf{r}, \mathbf{r}_s, \omega\right) \partial_i \tilde{G}_{ni}\left(\mathbf{r}, \mathbf{r}_g, \omega\right) \tilde{u}_i^*\left(\mathbf{r}, \mathbf{r}_s, \omega\right) \tilde{G}_{ni}^*(\mathbf{r}, \mathbf{r}_g, \omega).
\end{aligned} \tag{16}$$

According to equations (15) and (16), the multi-parameter approximate Hessian $\tilde{\mathbf{H}}$ and its parameter-type approximation $\tilde{\mathbb{H}}$ can be constructed using adjoint-state technique. The expressions of multi-parameter approximate Hessian and the parameter-type approximation for other elastic parameterizations can also be obtained using chain rule.

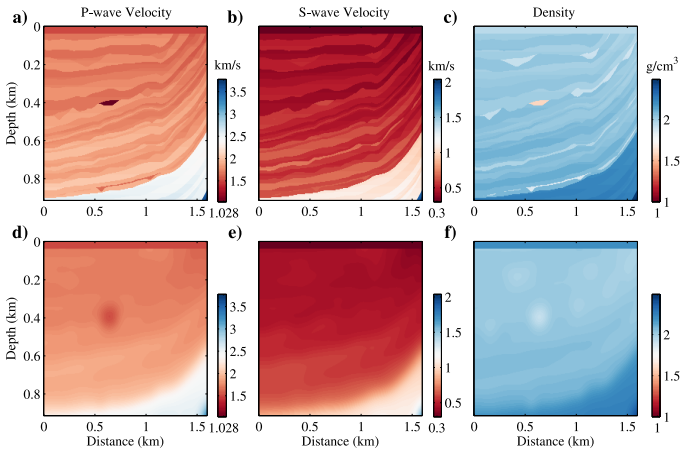

FIG. 6. (a), (b) and (c) show the true P-wave velocity, S-wave velocity and density model. (d), (e) and (f) show the initial P-wave velocity, S-wave velocity and density model.

NUMERICAL EXPERIMENTS

De-coupling the elastic parameters: a multi-scatter example

In this section, we first give a multi-scatter example to show that the ability of multi-parameter approximate Hessian $\tilde{\mathbf{H}}$ and its parameter-type approximation $\tilde{\mathbb{H}}$ in suppressing cross-talk. The initial model for inversion is a homogeneous and isotropic model with P-wave velocity $\alpha = 2500$ m/s, S-wave velocity $\beta = 1300$ m/s and density $\rho = 2.2$ g/cm^3. It consists of $50 \times 50 = 2500$ nodes with grid size of 5 m in both horizontal and vertical dimensions. Nine point scatters are embedded in the background model with -10% model perturbations. The true model perturbations for parameters α, β and ρ are shown in Figures 2a, b and c respectively. The horizontal and vertical sources are located at $\mathbf{r}_s = (x = 125 \text{ m}, y = 0 \text{ m}, z = 0 \text{ m})$.

We, first, explicitly construct the multi-parameter approximate Hessian $\tilde{\mathbf{H}}^{\text{z}}_{\text{lame}}$ and $\tilde{\mathbf{H}}^{\text{z}}_{\text{vel}}$ for Lamé constants parameterization and velocity parameterization using recorded z component data, as shown in Figures 3 and 4. It can be observed that the elastic multi-parameter approximate Hessian is a square and symmetric matrix and the energy distributions in $\tilde{\mathbf{H}}^{\text{z}}_{\text{lame}}$ and $\tilde{\mathbf{H}}^{\text{z}}_{\text{vel}}$ are quite different, which is determined by the scattering patterns of these elastic parameters. We also notice that $\tilde{\mathbf{H}}^{\text{z}}_{\text{vel}}$ is dominated by its diagonal block $\tilde{\mathbf{H}}^{\text{z}}_{\beta\beta}$, which corresponds to the scattering pattern of S-wave velocity. This is because significant SV-SV scattering due to $\delta\beta$ will present when incorporating S-wave source.

To verify the effectiveness of the multi-parameter approximate Hessian and its parameter-type approximation in suppressing cross-talk, we choose velocity parameterization and use only z component data for inversion. We, first, use only the data residuals $\Delta\mathbf{d}_\alpha$ due to $\delta\alpha$ for inversion. The estimated model perturbations for α, β and ρ using steepest descent method are illustrated in the first row of Figure 5a. Only the estimated model perturbation $\delta\mathbf{m}_\alpha$ is right. The estimated model perturbations $\delta\mathbf{m}_\beta$ and $\delta\mathbf{m}_\rho$ are cross-talk artifacts. Furthermore, we notice that $\delta\mathbf{m}_\rho$ is very similar to $\delta\mathbf{m}_\alpha$, which is caused by the ambiguity of the scattering patterns between α and ρ. The second row show the estimated model per-

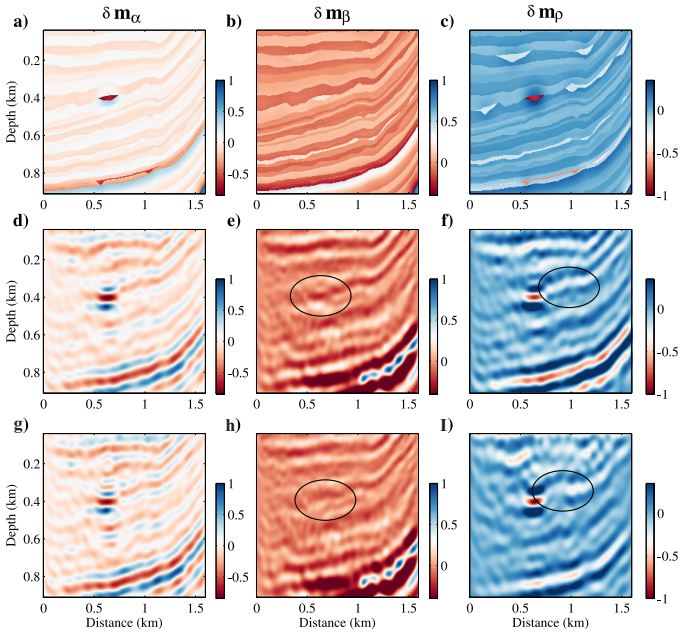

FIG. 7. (a), (b) and (c) show the true model perturbations $\delta\mathbf{m}_\alpha$, $\delta\mathbf{m}_\beta$ and $\delta\mathbf{m}_\rho$. (d), (e) and (f) show the estimated model perturbations preconditioned by the main diagonal elements of $\tilde{\mathbf{H}}$. (g), (h) and (i) show the estimated model perturbations preconditioned by the parameter-type approximation $\tilde{\mathbb{H}}$ (The amplitudes have been normalized).

turbations with parameter-type Hessian approximation preconditioning. The amplitudes in $\delta\mathbf{m}_\alpha$ have been scaled and the cross-talk artifacts in $\delta\mathbf{m}_\beta$ and $\delta\mathbf{m}_\rho$ are reduced obviously. The third row in Figure 5 show the estimated model perturbations with multi-parameter approximate Hessian $\tilde{\mathbf{H}}^z_{\text{vel}}$ preconditioning. $\delta\mathbf{m}_\alpha$ is obviously resolved. The artifacts in $\delta\mathbf{m}_\beta$ and $\delta\mathbf{m}_\rho$ are suppressed greatly. Figures 5b and c illustrate the estimated model perturbations using the data residuals $\Delta\mathbf{d}_\beta$ and $\Delta\mathbf{d}_\rho$. We can also observe the effectiveness of $\tilde{\mathbf{H}}$ and $\tilde{\mathbb{H}}$ in suppressing the cross-talk.

A Modified Marmousi-II Model Example

We then apply the parameter-type Hessian approximation preconditioning on a modified Marmousi-II model. Figures 6a, b and c show the true P-wave velocity, S-wave velocity and density. Figures 6d, e and f show the corresponding initial models. Figures 7a, b and c show the true model perturbations $\delta\mathbf{m}_\alpha$, $\delta\mathbf{m}_\beta$ and $\delta\mathbf{m}_\rho$ with normalized amplitudes. A total of 40 sources and 400 receivers are deployed along the top surface of the model. We construct the gradients and parameter-type approximation using a phase-encoding technique. Figures 7d, e and f show the corresponding gradients preconditioned by the main diagonal elements of $\tilde{\mathbf{H}}$ in the 1st iteration. The main diagonal elements of $\tilde{\mathbf{H}}$ can scale the gradients but cannot mitigate the cross-talk. Comparing Figures 7d, e and f with the true model perturbations, we can observe that P-wave velocity perturbation can be estimated very well. While some artifacts show up in the gradients for S-wave velocity and density, as indicated by the black circles. Figures 7g, h and i show the estimated model perturbations preconditioned by parameter-type approximation. We can observe that the artifacts are alleviated to

some extent.

CONCLUSIONS

In this research, we show that the multi-parameter approximate Hessian and its parameter-type approximation can be constructed using adjoint-state method efficiently. The parameter-type approximation preconditioning is then practiced on a multi-scatter example and a modified Marmousi-II example to verify its effectiveness in suppressing cross-talk.

ACKNOWLEDGEMENTS

The authors thank the sponsors of CREWES for continued support. This work was funded by CREWES industrial sponsors and NSERC (Natural Science and Engineering Research Council of Canada) through the grant CRDPJ 461179-13. Author 1 was also supported by a SEG/Chevron scholarship.

REFERENCES

Clayton, R. W., and Engquist, B., 1980, Absorbing boundary conditions for wave-equation migration: Geophysics, **45**, 895–904.

Epanomeritakis, I., Akçelik, V., Ghattas, O., and J.Bielak, 2008, A Newton-CG method for large-scale three-dimensional elastic full-waveform seismic inversion: Inverse Problems, **24**, 1–26.

Innanen, K. A., 2014a, Multicomponent elastic reflection full waveform inversion: CREWES Annual Report, 1–18.

Innanen, K. A., 2014b, Reconciling seismic avo and precritical reflection fwi-analysis of the inverse hessian: SEG Expanded Abstracts, 1022–1027.

Innanen, K. A., 2014c, Seismic avo and the inverse hessian in precritical reflection full waveform inversion: Geophysical Journal International, **199**, 717–734.

Köhn, D., Nil, D. D., Kurzmann, A., Przebindowska, A., and Bohlen, T., 2012, On the influence of model parameterization in elastic full waveform tomography: Geophysical Journal International, **191**, 325–345.

Lailly, P., 1983, The seismic inverse problem as a sequence of before stack migration: Conference on Inverse Scattering, Theory and Applications, SIAM, Expanded Abstracts, 206–220.

Levander, A. R., 1988, Fourth-order finite-difference p-sv seismograms: Geophysics, **53**, 1425–1436.

Mora, P., 1987, Nonlinear two-dimensional elastic inversion of multioffset seismic data: Geophysics, **52**, 1211–1228.

Operto, S., Gholami, Y., Prieux, V., Ribodetti, A., Brossier, R., Metivier, L., and Virieux, J., 2013, A guided tour of multiparameter full-waveform inversion with multicomponent data:from theory to practice: The Leading Edge, 1040–1054.

Pan, W., and Innanen, K. A., 2015, Scattering patterns in orthorhombic media: SEG Expanded Abstracts, submitted, 1–5.

Pan, W., Innanen, K. A., and Margrave, G. F., 2014a, A comparison of different scaling methods for least-squares migration/inversion: EAGE Expanded Abstracts.

Pan, W., Margrave, G. F., and Innanen, K. A., 2014b, Iterative modeling migration and inversion (immi): Combing full waveform inversion with standard inversion methodology: SEG Expanded Abstracts, 938–943.

Pratt, R. G., Shin, C., and Hicks, G. J., 1998, Gauss-newton and full newton methods in frequency-space seismic waveform inversion: Geophysical Journal International, **133**, 341–362.

Tarantola, A., 1984, Inversion of seismic reflection data in the acoustic approximation: Geophysics, **49**, 1259–1266.

Tarantola, A., 1986, A strategy for nonlinear elastic inversion of seismic reflection data: Geophysics, **51**, 1893–1903.

Tarantola, A., Fosse, I., Mendes, M., and Nercessian, A., 1985, The choice of model parameters for linearized elastic inversion of seismic reflection data,tech.rep.,equipe de tomographie du geophys., inst. de paris du globe, **2**, 325–345.

Virieux, A., and Operto, S., 2009, An overview of full-waveform inversion in exploration geophysics: Geophysics, **74**, WCC1–WCC26.

Virieux, J., 1986, P-sv wave propagation in heterogeneous media: Geophysics, **51**, 889–901.

Xiong, J., Abubakar, A., Lin, Y., and Habashy, T. M., 2011, 2.5D forward and inverse modelling of elastic full-waveform seismic data: SEG Expanded Abstracts, 2395–2400.